

**Sulfur Implanted Black Silicon for Metal Semiconductor
Metal (MSM) Photodetectors**

by Fred Semendy, Greg Meissner, and Priyalal Wijewarnasuriya

ARL-TR-6260

December 2012

NOTICES

Disclaimers

The findings in this report are not to be construed as an official Department of the Army position unless so designated by other authorized documents.

Citation of manufacturer's or trade names does not constitute an official endorsement or approval of the use thereof.

Destroy this report when it is no longer needed. Do not return it to the originator.

Army Research Laboratory

Adelphi, MD 20783-1197

ARL-TR-6260

December 2012

Sulfur Implanted Black Silicon for Metal Semiconductor Metal (MSM) Photodetectors

Fred Semendy, Greg Meissner, and Priyalal Wijewarnasuriya
Sensors and Electron Devices Directorate, ARL

REPORT DOCUMENTATION PAGE

Form Approved
OMB No. 0704-0188

Public reporting burden for this collection of information is estimated to average 1 hour per response, including the time for reviewing instructions, searching existing data sources, gathering and maintaining the data needed, and completing and reviewing the collection information. Send comments regarding this burden estimate or any other aspect of this collection of information, including suggestions for reducing the burden, to Department of Defense, Washington Headquarters Services, Directorate for Information Operations and Reports (0704-0188), 1215 Jefferson Davis Highway, Suite 1204, Arlington, VA 22202-4302. Respondents should be aware that notwithstanding any other provision of law, no person shall be subject to any penalty for failing to comply with a collection of information if it does not display a currently valid OMB control number.

PLEASE DO NOT RETURN YOUR FORM TO THE ABOVE ADDRESS.

1. REPORT DATE (DD-MM-YYYY) December 2012		2. REPORT TYPE Final		3. DATES COVERED (From - To)	
4. TITLE AND SUBTITLE Sulfur Implanted Black Silicon for Metal Semiconductor Metal (MSM) Photodetectors				5a. CONTRACT NUMBER	
				5b. GRANT NUMBER	
				5c. PROGRAM ELEMENT NUMBER	
6. AUTHOR(S) Fred Semendy, Greg Meissner, and Priyalal Wijewarnasuriya				5d. PROJECT NUMBER	
				5e. TASK NUMBER	
				5f. WORK UNIT NUMBER	
7. PERFORMING ORGANIZATION NAME(S) AND ADDRESS(ES) U.S. Army Research Laboratory ATTN: RDRL-SEE-I 2800 Powder Mill Road Adelphi, MD 20783-1197				8. PERFORMING ORGANIZATION REPORT NUMBER ARL-TR-6260	
9. SPONSORING/MONITORING AGENCY NAME(S) AND ADDRESS(ES)				10. SPONSOR/MONITOR'S ACRONYM(S)	
				11. SPONSOR/MONITOR'S REPORT NUMBER(S)	
12. DISTRIBUTION/AVAILABILITY STATEMENT Approved for public release; distribution unlimited.					
13. SUPPLEMENTARY NOTES					
14. ABSTRACT We have investigated a wet chemical process for nanoscale texturing of sulfur-doped silicon (Si) surfaces, which results in substantial suppression of the reflectivity in a broad spectral range, leading to black Si surfaces. The blackened surface was characterized optically and with Veeco micro-profiler. We fabricated metal semiconductor metal (MSM) test devices using the aforementioned black silicon and electrically characterized them for current-voltage (I-V), optical response, zero biased quantum efficiency (QE), and optical responsivity. We observe increased optical response and responsivity for the blackened silicon. One key observation we have made is the extension of the detectivity up to 1.2 μm, which is beyond 1.1 μm for a typical silicon detector. This observation was made under zero bias to the detector. We conclude that annealing and metal enhanced chemical etching (MECE) treatment prior to fabrication of the devices have enhanced the detectivity of the devices beyond the typical bandgap of 1.1 μm of silicon					
15. SUBJECT TERMS Metal Semiconductor Metals, Black Si, quantum efficiency					
16. SECURITY CLASSIFICATION OF:			17. LIMITATION OF ABSTRACT UU	18. NUMBER OF PAGES 18	19a. NAME OF RESPONSIBLE PERSON Fred Semendy
a. REPORT Unclassified	b. ABSTRACT Unclassified	c. THIS PAGE Unclassified			19b. TELEPHONE NUMBER (Include area code) (301) 394-4627

Contents

List of Figures	iv
1. Introduction	1
2. Experimental Setup	2
3. Result and Discussion	4
4. Conclusion	9
5. References	10
List of Symbols, Abbreviations, and Acronyms	11
Distribution List	12

List of Figures

Figure 1. MSM detector on MECE np Si sample (a) top view of ion implanted photodiode showing the interdigitated pattern of the top metal contacts. (b) Cross-sectional schematic diagram of the diode.	2
Figure 2. Depiction of the beam splitter and its effect on the optical beam and beam path.	3
Figure 3. Depth profile of sulfur implanted sample by SIMS.	4
Figure 4. Profiling of the MECE processed np SI sample (a) shows the surface from the top. (b) Surface scan in the x - and y -directions, which shows the presence of nanoscale pillars with a depth of ~ 5 nm.	5
Figure 5. The reflection spectra of the treated and MECE treated np Si.	5
Figure 6. I-V of 2.35×10^{14} sulfur/cm ² doped and unannealed MSM photodiode (a) I-V with no light and with light and (b) of the same dark current with and without light for unannealed sample.	6
Figure 7. I-V of sulfur-doped np Si, which was MECE treated: (a) sample with varying power of light and without light and (b) the dark current of the sample with and without light.	7
Figure 8. I-V of sulfur-doped np Si, which was MECE treated and annealed: (a) sample with varying power of light and without light and (b) dark current of the sample of the sample with and without light for 450 and 550 °C annealed samples.	7
Figure 9. EQE and responsivity of MECE treated and annealed at 450 °C samples with MSM detectors with zero bias. Sample size 3.5×10^{-5} cm ² for a IQE 200 beam size of 1 mm \times 2.5 mm.	8

1. Introduction

Significant interest has been shown in recent years in the optical and electrical properties of laser-microstructured chalcogen-laden silicon (Si), which shows enhanced optical absorption at wavelengths above and below the band gap (1, 2). A less cumbersome technique, namely, metal enhanced chemical etching (MECE) was used to create Si and further fabrication of devices (3, 4). In these papers, the authors developed and used a simple wet chemical etching technique to completely suppress the reflectivity in a broad spectral range, leading to a black surface Si.

Si with various structural morphologies is widely used for solar cells and other optoelectronic devices. Flat Si surfaces have a high natural reflectivity with a strong spectral dependence. The minimization of reflection losses is of crucial importance, in particular, for high efficiency solar cells, and hence, a variety of approaches has been developed to this end, in many cases specific to a particular surface morphology. One way to reduce the antireflection is by using antireflection coating (ARC). Alternatively, ARCs from oxidized nano-porous Si can be formed by electrochemical etching (5) Such coatings are resonant structures and perform well only in a limited spectral range and for specific angles of incidence. Their typical net effect in the entire usable spectral range of Si is an average reduction of the surface reflection to about 8–15%. Efficient suppression of reflection in a broad spectral range has been also achieved by deep surface texturing using reactive ion etching techniques in the past (6).

The black Si was produced for the first time during the formation of Si trenches by reactive ion etching (RIE) in fluorine, bromine, and chlorine plasmas (7). Also, it can be formed by a maskless RIE employing tetrafluoromethane (CF_4) (8) due to auto-masking of the surface at random spots. However, the detailed mechanism of black Si formation and the origin of its properties are yet to be understood. It is widely believed that the formation of nanopillars during RIE is due to a local variation of the Si etch rate. This variation in etching rate can be caused by Si surface itself, for example, inhomogeneous oxide layer or incompletely removed native oxide. The plasma tool and plasma source can be a cause of a micro-masking material, e.g., by-products of sputtering and redeposition of plasma chamber electrodes and masking.

In recent years, laser-microstructured chalcogen-laden, reflectivity reduced Si was used to fabricate Si-based electronic and optoelectronic devices. Such material is synthesized by repeated femto- or nanosecond laser irradiation of Si wafers in sulfur hexafluoride (SF_6), leading to sulfur-laden disordered Si layers with about 10- μm -tall spikes (9, 10). Similar work was also done with ion implantation followed by pulsed laser melting (11, 12) and pulsed laser mixing (13). The laser-shined materials with chalcogen, in general, showed increased absorption of sub-bandgap infrared photons. They also studied the usage of materials for potential application as photo-detectors (14) and photovoltaics (15).

Here, we report a simple p Si with a thin layer of sulfur implantation at the top followed by MECE of the implanted region, which creates black Si with suppressed reflectivity and increased absorption. In addition, the material was annealed at different temperatures prior to MECE treatment to gain knowledge on the effect of annealing. The etched samples were used to fabricate metal semiconductor metal (MSM) detectors to evaluate the optical and electrical properties.

2. Experimental Setup

For the experiment, we used a 300- μm -thick, double-side-polished p-type that was *B* doped, with a resistivity of 5–10 $\Omega\text{ cm}$, and doping level of $1.0 \times 10^{15}\text{ cm}^{-3}$. The wafer was ion implanted at the top layer at room temperature with 300 keV 32S^+ to doses ranging from 1×10^{14} to 1×10^{16} ions/ cm^2 . Evans Analytical Group (EAG) measured the implanted depth of the sulfur using secondary ion mass spectroscopy (SIMS). An implanted wafer was scribed into a number of pieces for MECE processing as per the procedure of MECE as explained in references 3 and 4. Samples were cleaned after the chemical etching, and used for optical studies and device fabrication. Optical measurements were carried out using Perkin Elmer Lambda 950 ultraviolet (UV)-Visible spectrometer for % transmittance and % reflection. Absorption was calculated using the formula:

$$\text{Absorption} = 1 - (\% \text{ transmittance} + \% \text{ reflectance}) \quad (1)$$

Some of the etched samples were used to fabricate MSM photodetectors using standard photolithography. A fabricated device is shown on figure 1. Titanium (Ti)/gold (Au) (200/2500 \AA) was used for metal contacts. Current-voltage (I-V) measurements on the on the pn junction were performed at room temperature. For optical response measurements, broad light source with varying power level was used.

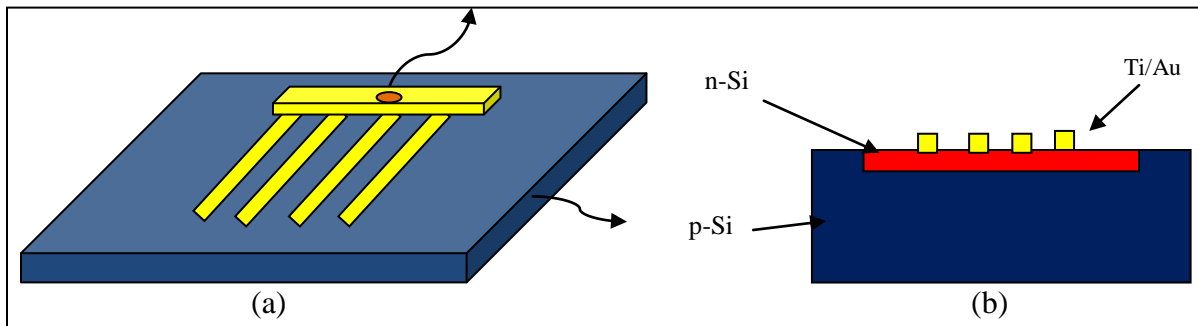


Figure 1. MSM detector on MECE np Si sample (a) top view of ion implanted photodiode showing the interdigitated pattern of the top metal contacts. (b) Cross-sectional schematic diagram of the diode.

Fabricated devices were used for I-V measurements as well as optical response studies using a calibrated broad band light source. Samples were also annealed at 450, 550, 650, and 750 $^{\circ}\text{C}$ and

were MECE treated prior to the fabrication of the MSM devices. The goal here was to observe the effect of annealing on the response current.

We used Oriel IQE- 200 EQE/IQE measurement for extended wavelength range to measure the quantum efficiency (QE). The IQE 200 incorporates a novel geometry that splits the beam, allowing for simultaneous measurement of external quantum efficiency (EQE) and the reflective losses to quantify internal quantum efficiency (IQE). The power spectral responsivity $R_{pa}(\lambda)$, for collected electrons per incident photons may be converted to external QE (λ), and then to internal quantum efficiency IQE (λ), using the equations,

$$QE(\lambda) = \frac{hc}{q} \frac{R_{pa}(\lambda)}{\lambda} \quad (2)$$

$$IQE(\lambda) = \frac{QE(\lambda)}{1 - R_{sample}(\lambda)} \quad (3)$$

where $R_{sample}(\lambda)$ is effective sample reflectance.

The optical layout of the beam splitter in the IQE 200 system is illustrated in figure 2.

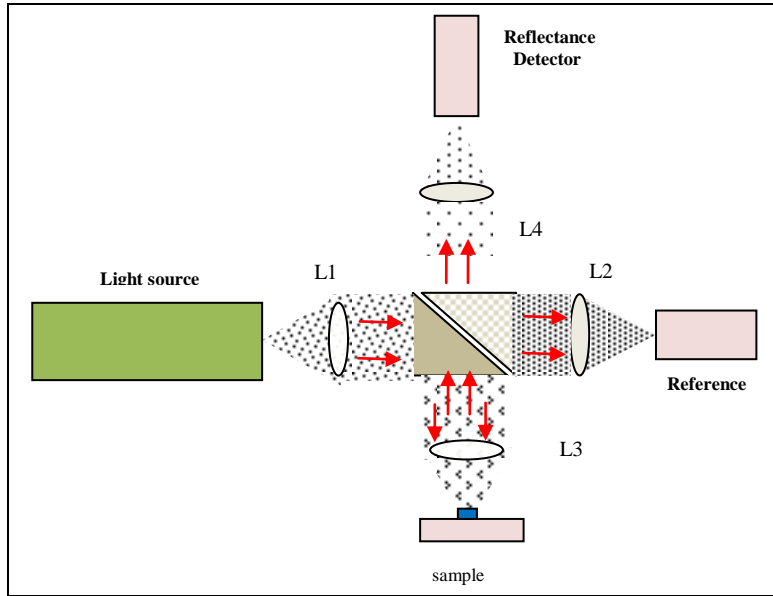


Figure 2. Depiction of the beam splitter and its effect on the optical beam and beam path.

It is comprised of one spectrally neutral 50-50 beam splitter and four lenses. The output light from the monochromator is first collimated by lens 1. The collimated light is then split into two beams of which one passes through the beam splitter and is focused by lens 2 onto the reference detector. This detector measures the output light of any given wavelength. The other beam is reflected by the beam splitter down onto sample surface through focusing lens 3 for the QE measurement. The spot size on the sample is determined by the lens 3. Therefore, by varying lens 3 optical parameters a variety of spot size options can be obtained. For the IQE

measurement, the reflected light from the sample is collimated lens 3 and then a known factor of it passes through the beam splitter. The beam is then focused by lens 4 on to the reflectance detector.

3. Result and Discussion

Figure 3 gives the SIMS analysis results of the sulfurimplanted p-type Si. It is clearly seen that the maximum concentration of sulfur is around 0.4 μm with a concentration of $1 \times 10^{19} \text{ cm}^{-3}$ and the lowest is around 1.1 μm with a sulfur concentration of $1 \times 10^{16} \text{ cm}^{-3}$, which gives an n-type layer with thickness of about 1.1 μm with varying sulfur concentration and an average concentration of $1 \times 10^{17} \text{ cm}^{-3}$.

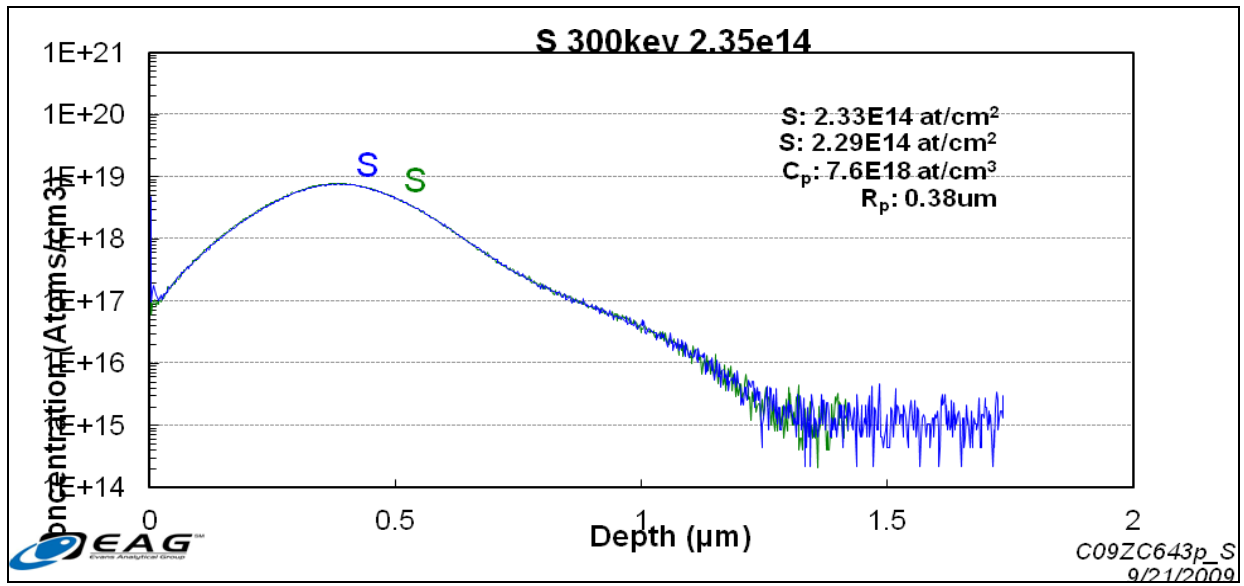


Figure 3. Depth profile of sulfur implanted sample by SIMS.

The surface of the MECE processed samples was characterized by the Veeco profilometer. The top view of the scan is depicted in figure 4a, which gives the root mean square (rms) value of 1.24 nm. The sample under consideration was etched for 5 min using the MECE technique. Figure 4b gives the surface scan of the sample, which shows the x - and y -direction scans and the presence of spiked nanoscale pillars. The depth is of the order of ~ 5 nm on the average with rms value of 1.8 nm in both directions.

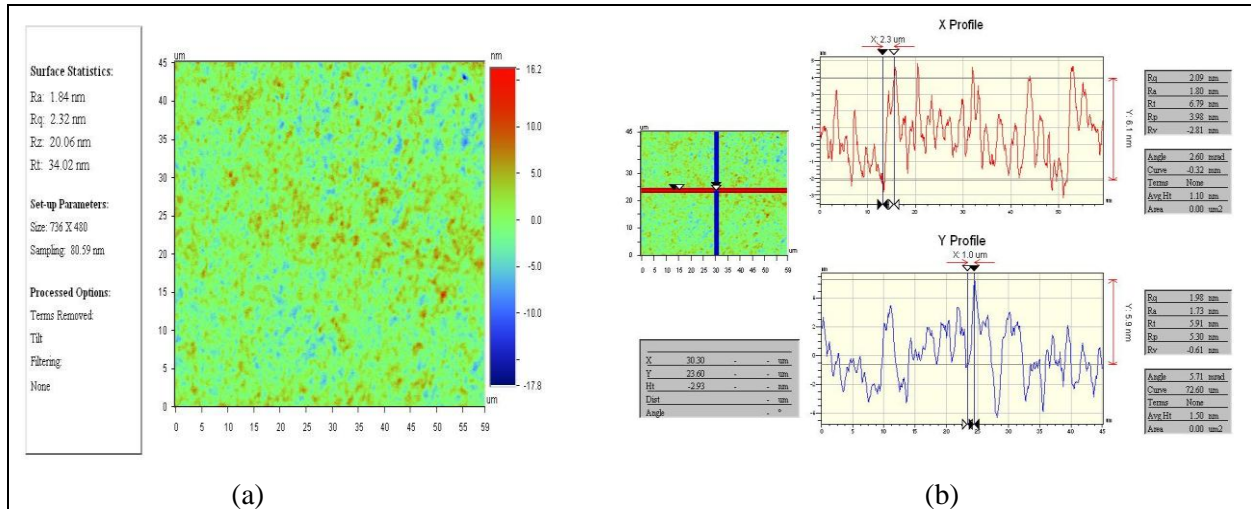


Figure 4. Profiling of the MECE processed np Si sample (a) shows the surface from the top. (b) Surface scan in the x- and y-directions, which shows the presence of nanoscale pillars with a depth of ~5 nm.

In figure 4, the depth of the pillars are in the order of ~5 nm on the average with rms value of 1.8 nm in both directions. This result proves that the MECE processing has created nanopillars on the surface of the np Si, which will trap the light when it falls on the surface, making it look black. The % reflection spectra of the treated and MECE treated np-silicon is plotted in figure 5.

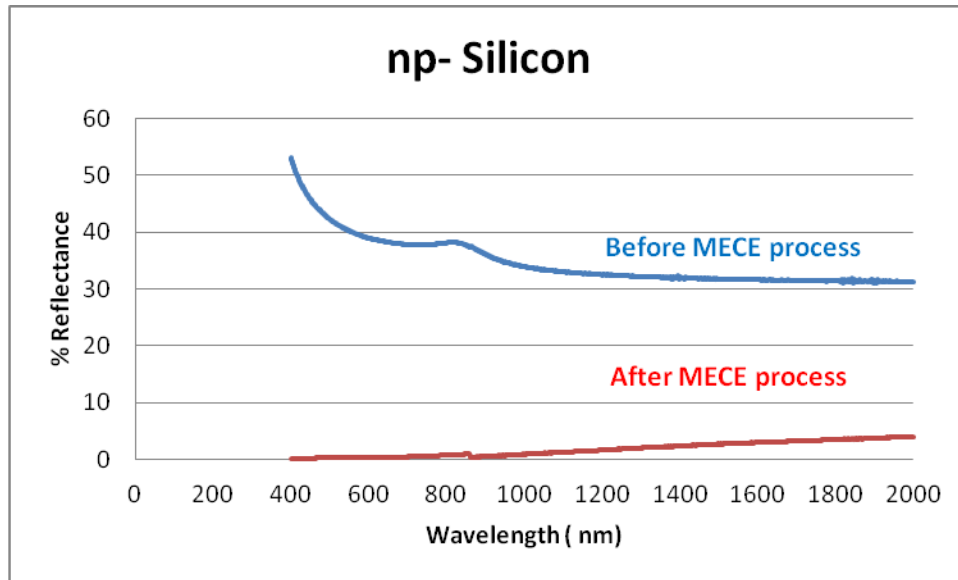


Figure 5. The reflection spectra of the treated and MECE treated np Si.

The % reflection of the untreated samples is about 30–50% for the spectral region of 400–2000 nm, where it is substantially reduced for the samples that were MECE treated on the front side, as seen in figure 5. We have observed that the % transmission increased when the % reflectivity decreased for the treated samples.

A set of samples were annealed, MECE treated followed by the fabrication of MSM devices. The intention here was to find the effects of annealing and chemical etching on the optical response of the detectors. Rapid thermal annealing (RTA) was carried out for 30 min in nitrogen atmosphere. Annealing was carried out for 450, 550, 650, and 750 °C. Once the annealing was complete, MECE was carried out as explained in references 3 and 4. Annealed and MECE treated, and unannealed and MECE treated samples were separately used to fabricate the MSM photodetectors using standard lithographic techniques. Fabricated devices were used for I-V measurements and the results are shown in figures 6, 7, and 8. Figure 6 give the dark current of the unannealed and untreated MSM detector with and without light.

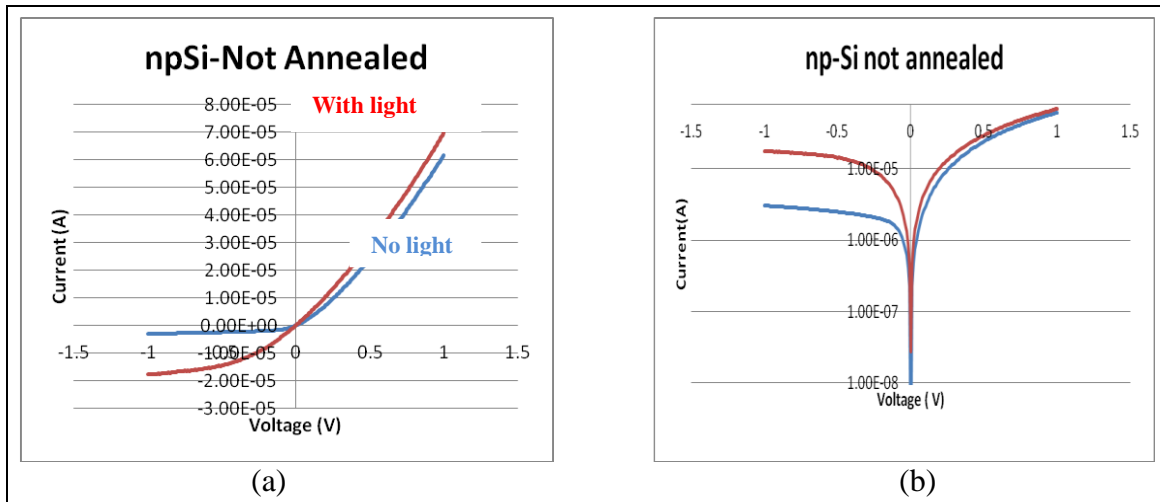


Figure 6. I-V of 2.35×10^{14} sulfur/cm² doped and unannealed MSM photodiode (a) I-V with no light and with light and (b) of the same dark current with and without light for an unannealed sample.

Figure 7 gives the I-V of sulfur-doped np Si without annealing but MECE treated for (a) a sample with varying power of light and without light and (b) shows the dark current of the sample with and without light. Comparing the results in figures 6 and 7, one can see the clear difference in the increased response current in the case of the MECE-treated sample, indicating the effect of reduced reflectivity and increase absorption of photons.

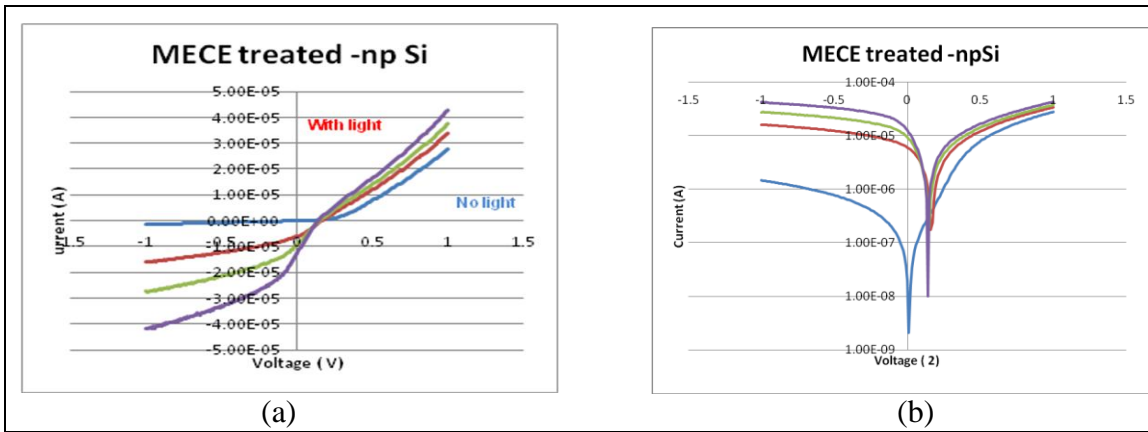


Figure 7. I-V of sulfur-doped np Si, which was MECE treated: (a) sample with varying power of light and without light and (b) the dark current of the sample with and without light.

Figure 8 gives the case where all the samples were annealed and MECE treated prior to fabrication of the devices. There is evidence of increased photocurrent in annealed and etched samples. All curves show good rectifying behavior when the I-V is measured without light. Higher temperature annealed samples show increased short circuit current as well as increased in open circuit voltage. However, further increase in annealing temperature did not increase either of these two, but we observed a decrease in both. The increased short circuit current and open circuit voltage can be attributed to the decrease in the density of point defects. It is anticipated that at higher temperature excessive clustering of the sulfur dopants can occur, thereby degrading the electrical properties of the junctions. Obviously, the annealing temperature has a role to play in the photovoltaic behavior of the junctions.

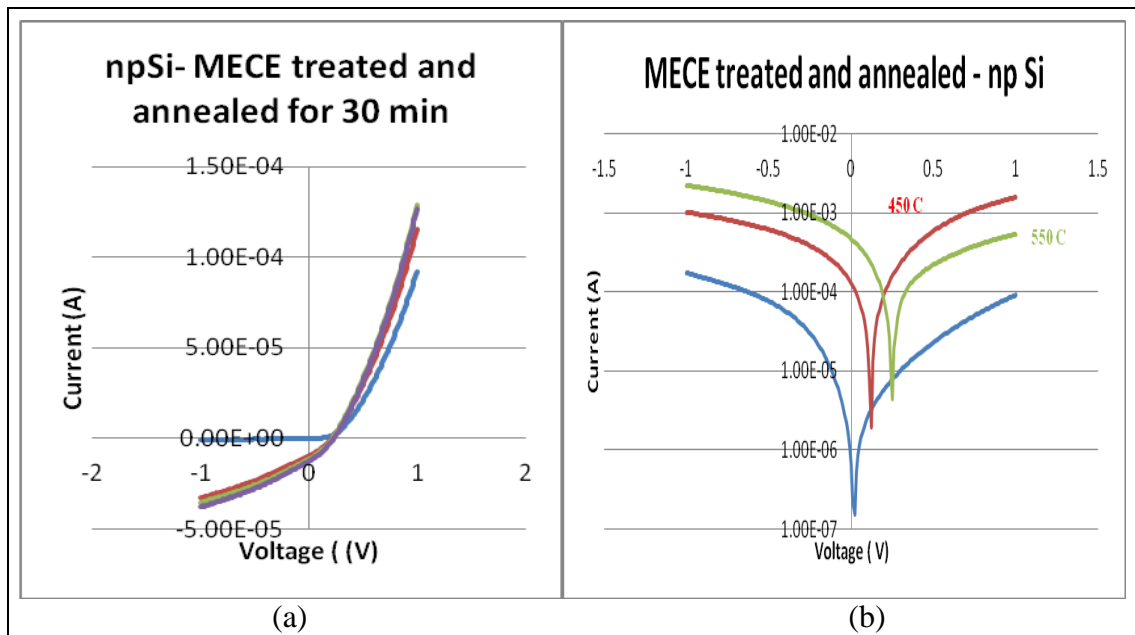


Figure 8. I-V of sulfur-doped np Si, which was MECE treated and annealed: (a) sample with varying power of light and without light and (b) dark current of the sample of the sample with and without light for 450 and 550 °C annealed samples.

Figure 8 indicates the results for 450 and 550 °C. It is anticipated the mobility of the carriers has significantly enhanced for the annealed samples compared to the unannealed samples. Annealing may also enable the evolution of inactive point defects from a charged to a neutral configuration, thereby reducing the scattering probability of the free carriers (16).

The QE and responsivity of the device were measured. The beam size was 1 mm × 2.5 mm and was positioned in the system to provide the maximum illumination and photoresponse for the device. The system was used for the calibration of commercially available Si and an indium gallium arsenide (InGaAs) photodiodes and compared with the manufacturer’s calibration curves. The interdigitated finger type MSM had an active area of $3.5 \times 10^{-5} \text{ cm}^2$. The monochromatic light was chopped and the response could be measured using a lock-in amplifier. Results of the QE and responsivity are plotted on figure 9. Highest intensity occurred beyond 600 nm; however, there was a drop in the response at 720 nm due to detector change. One observation we have made is the extension of the detectivity beyond 1.1 μm for a typical Si detector for zero bias. Said and others have observed similar behavior for laser-shined np Si beyond 1.1 μm with increasing gain effect with increased bias voltage (17). We conclude that that our inhouse developed low-cost annealing and MECE treatment prior to fabrication of the devices have enhanced the detectivity of the devices to 1.2 μm beyond the typical bandgap 1.1 μm of Si

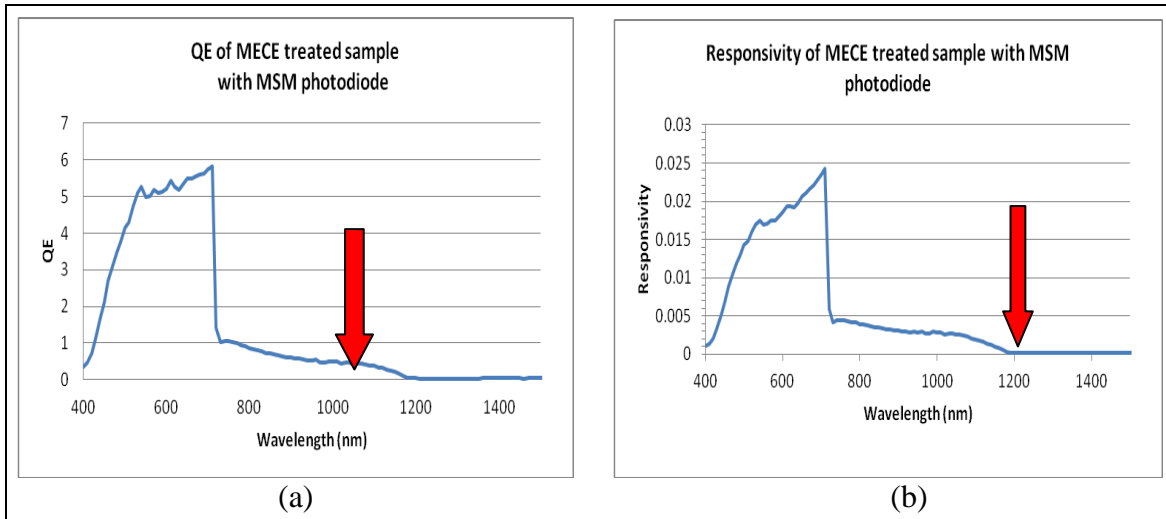


Figure 9. EQE and responsivity of MECE treated and annealed at 450 °C samples with MSM detectors with zero bias. Sample size $3.5 \times 10^{-5} \text{ cm}^2$ for a IQE 200 beam size of 1 mm × 2.5 mm.

4. Conclusion

In summary, we have doped a thin layer of n-type Si with sulfur by ion implantation technique to create an np-Si structure. The material was annealed at various temperature followed by an in house developed MECE treatment. MSM photodiodes were fabricated for photoresponse studies. The diodes showed good and varying photoresponse for annealed samples of different temperatures. Data show good rectifying behavior when the I-V is measured without light. High temperature annealed samples show increased short circuit current as well as increased open circuit voltage. However, further increase in the annealing temperature did not increase either of the two, but rather demonstrated a decrease. The increased short circuit current and open circuit voltage can be attributed the decrease in the density of point defects. It is anticipated that at higher temperature, excessive clustering of the sulfur dopants can occur, thereby degrading the electrical properties of the junctions. Obviously, the annealing temperature has a role to play in the photovoltaic behavior of the junctions. The QE and responsivity of the device were measured. One major observation we have made is the extension of the detectivity to 1.2 μm , which is beyond 1.1 μm for a typical Si detector for zero bias. We conclude that annealing and MECE treatment prior to fabrication of the devices have enhanced the detectivity of the devices beyond the typical bandgap of 1.1 μm of Si.

5. References

1. Crouch, C. H.; Carey, J. E.; Warrender, J. M.; Mazur, E.; Aziz, M. J.; Genin, F. *Appl. Phys. Lett.* **2004**, *84*, 1850.
2. Wu, C.; Crouch, C. H.; Younkin, R.; Zhao, L.; Carey, J. E.; Younkin, R.; Levinson, J.; Mazur, E.; Farrell, R. M.; Gothoskar, P.; Karger, A. *Appl. Phys. Lett.* **2001**, *78*, 1850.
3. Koynov, S.; Brandt, M. S.; Stutzman, M. *Appl. Phys. Lett.* **2006**, *88*, 20317.
4. Semendy, F.; Taylor, P.; Meissner, G.; Wijewarnasuriya, P. *MSM-Metal Semiconductor Metal Photo-detector Using Black Silicon Germanium (SiGe) for Extended Wavelength Near Infrared Detection*; ARL-TR-6176; U.S. Army Research Laboratory: Adelphi, MD, 2012.
5. Prasad, A.; Balakrishnan, S.; Jain, S. K.; Jain, C. G. *J. Electrochem.Soc.* **1995**, *129*, 596.
6. Green, M. A. *Silicon Solar Cells: Advanced Principles and practice* (Bridge, Sydney, 1995).
7. Oerlein, G. S.; Rembetski, J. F.; Payne, E. H. *J. Vac. Sci. Technol.* **1990**, *B8*, 1199.
8. Gharghi M.; Sivaththaman S. *J. Vac. Sci. Technol. A* **2006**, *24*, 723.
9. Crouch, C. H.; Carey, J. E.; Shen, M.; Mazur, E.; Aziz, M. J.; Genin, F. *Appl. Phys. A: Mater. Sci. Process.* **2004**, *79*, 1635.
10. Petraza, A. J.; Fowlkes, J. D.; Lowndes, D. H. *Appl. Phys. Lett.* **1999**, *74*, 2322.
11. Kim, T. G.; Warrender, J. M.; Aziz, M. A. *Appl. Phys. Lett.* **2006**, *88*, 241902.
12. Tabbal, M.; Kim, T.; Warrender, J. M.; Aziz, M. J.; Cardozo, B. L.; Goldman, R. S. *J. Vac. Sci. Technol.* **2007**, *B25*, 1847.
13. Tabbal, M.; Kim, T.; Woolf, D. N.; Shin, B.; Aziz, M. J. *Appl. Phys A* **2010**, *98*, 589.
14. Huang, Z.; Carey, J. E.; Liu, M.; Guo, X.; Mazur, E.; Campbell, J. C. *Appl. Phys. Lett.* **2011**, *89*, 033506.
15. Pan, S. H.; Recht, D.; Charnvanichborikarm, S.; Williams, J. S.; Aziz, M. J. *Appl. Phys. Lett.* **2011**, *98*, 121913.
16. Takamura, Y.; Jain, S. H.; Griffin, P. B.; Plummer, J. D. *J Appl. Phys* **2002**, *92*, 230.
17. Said, A. J.; Recht, D.; Sullivan, J. T.; Warrender, J. M.; Buonassisi, T.; Parsans, P. D.; Aziz, M. J. *Appl. Phys. Lett.* **2011**, *99*, 073503.

List of Symbols, Abbreviations, and Acronyms

ARC	antireflection coating
Au	gold
CF ₄	tetrafluoromethane
EAG	Evans Analytical Group
EQE	external quantum efficiency
InGaAs	indium gallium arsenide
IQE	internal quantum efficiency
I-V	current-voltage
MECE	metal enhanced chemical etching
MSM	metal semiconductor metal
QE	quantum efficiency
RIE	reactive ion etching
rms	root mean square
SF ₆	sulfur hexafluoride
Si	silicon
SIMS	secondary ion mass spectroscopy
Ti	titanium
UV	ultraviolet

1 DEFENSE TECHNICAL
(PDF INFORMATION CTR
only) DTIC OCA
8725 JOHN J KINGMAN RD
STE 0944
FORT BELVOIR VA 22060-6218

1 DIRECTOR
US ARMY RESEARCH LAB
IMAL HRA
2800 POWDER MILL RD
ADELPHI MD 20783-1197

1 DIRECTOR
US ARMY RESEARCH LAB
RDRL CIO LL
2800 POWDER MILL RD
ADELPHI MD 20783-1197

1 DIRECTOR
US ARMY RESEARCH LAB
RDRL CIO LT
2800 POWDER MILL RD
ADELPHI MD 20783-1197

2 DIRECTOR
US ARMY RESEARCH LAB
RDRL SEE
RDRL SEE I
2800 POWDER MILL RD
ADELPHI MD 20783-1197